

# UNSEEN trends: Detecting decadal changes in 100-year precipitation extremes

T. Kelder<sup>1,2\*</sup>, M. Müller<sup>2,3</sup>, L.J. Slater<sup>4</sup>, T.I. Marjoribanks<sup>5</sup>, R.L. Wilby<sup>1</sup>, C. Prudhomme<sup>6,7</sup>, P. Bohlinger<sup>2</sup>,  
L. Ferranti<sup>6</sup>, T. Nipen<sup>2</sup>

<sup>1</sup>Geography and Environment, Loughborough University, Loughborough, UK

<sup>2</sup>The Norwegian Meteorological Institute, Oslo, Norway

<sup>3</sup>Section for Meteorology and Oceanography, Department of Geosciences, University of Oslo,  
Norway

<sup>4</sup>School of Geography and the Environment, University of Oxford, Oxford, UK

<sup>5</sup>School of Architecture, Building and Civil Engineering, Loughborough, UK

<sup>6</sup>European Centre for Medium-Range Weather Forecasts (ECMWF), Reading, UK

<sup>7</sup>Centre for Ecology and Hydrology, Wallingford, UK

\* [T.Kelder@lboro.ac.uk](mailto:T.Kelder@lboro.ac.uk)

This paper is a non-peer reviewed preprint submitted to *NPJ Climate and Atmospheric Science*.

**Sample sizes of observed climate extremes are typically too small to reliably constrain non-stationary behaviour. To facilitate detection of non-stationarities in 100-year precipitation values over a short period of 35 years (1981-2015), we apply the UNprecedented Simulated Extreme ENsemble (UNSEEN) approach, by pooling ensemble members and lead times from the ECMWF seasonal prediction system SEAS5. We generate a 3500-year UNSEEN dataset of autumn 3-day extreme precipitation events across Western Norway and Svalbard. The UNSEEN ensemble shows that an event of 1.5 times the magnitude of the most severe flood episode recorded in Western Norway can arise with a return period of ~2000 years. Applying the novel UNSEEN-trends approach, we demonstrate that for Svalbard the 100-year event in 1981 could be expected to occur with a return period of around 40 years in 2015. These new insights have important implications for current design-level practices and for understanding the underlying causes of non-stationarities.**

Handling the non-stationarity of climate extremes is an active area of research<sup>1-3</sup> that is confounded by the brevity and sparsity of observational records<sup>4-6</sup>. Non-stationary precipitation analyses typically focus on detecting multidecadal to centennial changes in annual precipitation maxima<sup>7-9</sup>. However, annual maximum precipitation events do not necessarily cause high impacts and hence, a

33 potentially more pressing research challenge is the detection of changes in larger extremes<sup>10,11</sup>, such  
34 as the 1-in-100-year event. Furthermore, the impacts of abrupt warming in recent decades may not  
35 yet be detectable in short precipitation records. Therefore, robust detection of short-term (decadal,  
36 rather than centennial) trends in climate extremes may provide valuable and actionable information.

37 An emerging alternative to traditional observation-based extreme value analysis is to pool ensemble  
38 members from numerical weather prediction systems<sup>12–22</sup> – the UNprecedented Simulated Extreme  
39 ENsemble (UNSEEN) approach<sup>20,22</sup>. This technique creates numerous alternative pathways of reality,  
40 thus increasing the event sample size for statistical analysis. The larger sample size offers a broader  
41 view of present-day hazard and, therefore, has potential to improve design-levels. For example, the  
42 2013/14 winter flooding in the UK had no observational precedent, but could have been anticipated  
43 with the UNSEEN approach<sup>22</sup>. Similarly, estimates of storm surge levels of the River Rhine<sup>12,13</sup>, global  
44 ocean wind and wave extremes<sup>15,16,18</sup>, and losses from extreme windstorms<sup>19</sup> have all been improved  
45 with the UNSEEN approach. UNSEEN can also enhance food security through better drought  
46 exposure estimates<sup>14,21</sup> and can assist policy makers and contingency planners by quantifying and  
47 explaining the most severe events possible in the current climate, such as heatwaves in China<sup>20</sup>.  
48 However, validating the UNSEEN method is a well-recognised difficulty in existing studies, and  
49 UNSEEN has not yet been used to facilitate detection of non-stationarity in climate extremes over  
50 short periods of several decades.

51 Here, we provide a framework to systematically evaluate the robustness of the UNSEEN approach  
52 and we present a novel UNSEEN-trends approach, where we aim to provide confident short-term  
53 trend estimates by using the larger event sample to better constrain changes in climate extremes.  
54 We do this in a storyline context<sup>23</sup>, where we take observed flood episodes as a starting point for our  
55 analysis. We select the west coast of Norway and the Svalbard Archipelago as study regions; two  
56 contrasting areas in terms of precipitation extremes. Western Norway faces the highest extremes  
57 within Europe<sup>24</sup> and has a dense station network<sup>25,26</sup>, whereas Svalbard is a semi-desert with only a  
58 few observation stations<sup>27</sup>. Both regions have faced severe damages from recent extreme events,  
59 such as the September 2005<sup>28</sup> and October 2014<sup>29</sup> floods over Western Norway and the slush-  
60 avalanche inducing extreme precipitation event over the Svalbard Archipelago in 2012<sup>30</sup>. The  
61 extreme events were driven by atmospheric rivers<sup>27–29</sup> (ARs), which cause heavy precipitation over a  
62 prolonged period. As AR-related floods predominantly occur in autumn and frequently strengthen  
63 over a period of several days<sup>28,29</sup>, we select autumn (September to November) spatial averaged  
64 (Supplementary fig. 1) three-day extreme precipitation (SON-3DP) as target events.

65 Previous UNSEEN studies have used the Hadley Centre global climate model, HadGEM3-GC2<sup>14,20–22</sup>  
66 and the European Centre for Medium-ranged Weather Forecasts (ECMWF) ensemble prediction  
67 systems<sup>15–18</sup> and earlier version of the seasonal prediction system<sup>12,13,19</sup>. Here, we are the first to use  
68 the latest ECMWF seasonal prediction system SEAS5<sup>31</sup> for its high-resolution, large ensemble, long  
69 homogeneous hindcast period (1981-2015) and open access. The ECMWF atmospheric model has  
70 shown skill in simulating atmospheric rivers for Northern Europe<sup>32</sup>, giving confidence in the realism  
71 of these extreme events in SEAS5, hence is a good candidate for the UNSEEN method. We use the 25  
72 ensemble members across lead times of 2-5 months, resulting in a sample of 100 members (called  
73 the UNSEEN ensemble) and evaluate the independence and stability of the pooled sample for SON-  
74 3DP events across Western Norway and Svalbard. We then use the UNSEEN-trends approach to  
75 identify unprecedented extreme precipitation events and to detect trends in 100-year precipitation  
76 events over the last 35 years. These findings will help understanding the robustness of current  
77 design levels and may improve our understanding of physical processes driving climate extremes and  
78 their non-stationarity.

#### 79 **Ensemble member independence and model stability**

80 The independence of ensemble members is an important requirement for the UNSEEN approach, as  
81 dependent members would artificially inflate the sample size, without adding new information.  
82 Previous studies have assessed the independence of ensemble members for lead times 9-10  
83 days<sup>15,16,18</sup>, but to the best of our knowledge, no independence test has yet been performed in  
84 UNSEEN studies of seasonal prediction systems.

85 For the regions studied here, the ensemble members from lead times beyond one month are not  
86 dependent on atmospheric initial conditions, because the synoptic patterns related to ARs are  
87 known not to be predictable beyond two weeks<sup>32,33</sup>. However, predictability on a seasonal timescale  
88 may be found through slowly varying components of the ocean-atmosphere system. Therefore,  
89 while the ensemble members might represent unique weather events because of the independency  
90 to the atmospheric initial conditions, the weather events could have a conditional bias induced by  
91 favourable conditions in the slowly varying components of the ocean-atmosphere system.

92 To test the seasonal dependence of SON-3DP, we first select the seasonal maximum event for each  
93 forecast then concatenating these events to create a 35-year timeseries (Fig. 1a,b,c). To robustly  
94 assess the independence between each of the ensemble members, we calculate the Spearman rank  
95 correlation coefficient ( $\rho$ ) for every distinct pair of ensemble members (Fig. 1d), resulting in 300  $\rho$   
96 values for each lead time. The value of  $\rho$  ranges from ca. -0.6 to 0.6, and the median correlation is  
97 close to zero for all lead times for both Western Norway and Svalbard (Fig. 1e,f). The range in  $\rho$

98 values is expected due to the large number of correlation tests, and none of the lead times fall  
99 outside the range that would be expected for uncorrelated data for the West Coast of Norway (Fig.  
100 1e). For Svalbard, slightly higher  $\rho$  values are found, with the median correlation still within the  
101 expected range, but the interquartile range just exceeding the upper boundary of the confidence  
102 intervals for the first two lead times (Fig. 1f). The small correlations found for Svalbard might be  
103 driven by the trend that we detect for this region (UNSEEN-trends section), and thus, the UNSEEN  
104 ensemble members represent unique events that follow the slowly evolving climate signal, as  
105 desired.

106 A second potential issue for generating the UNSEEN ensemble could be a drift in the simulated  
107 climatology<sup>34,35</sup>, which may alter precipitation extremes over longer lead times. Therefore, model  
108 stability is a requirement for pooling lead times. Model stability is assessed by comparing the  
109 distribution of predicted SON-3DP events across different lead times. For both regions, the  
110 probability density functions of the pooled SON-3DP events for the considered lead times are  
111 remarkably similar (Fig. 2a,b). Moreover, the empirical extreme value distributions of the individual  
112 lead times fall within the uncertainty range of the distribution of all lead times pooled together and  
113 thus, the model can be considered stable over lead times (Fig. 2c,d).

#### 114 **Fidelity of UNSEEN extremes for Western Norway**

115 Confidence in simulated 'unprecedented extremes' in large ensembles is complicated by the inability  
116 to validate extremes, given the limited sample sizes of observations. Here, we evaluate the UNSEEN  
117 ensemble with 1) rank histograms, commonly applied in ensemble forecast verification<sup>36</sup> and 2) by  
118 bootstrapping the ensemble into datasets of 35 years and assessing whether observations fall within  
119 the range of the bootstrapped distribution, following previous UNSEEN studies<sup>20,22</sup> (see Methods).  
120 We perform this analysis for the SEAS5 UNSEEN SON-3DP ensemble over Western Norway, because  
121 the dense station network of the country<sup>25,26</sup> facilitates model evaluation (unlike in Svalbard). For a  
122 comprehensive global model validation of SEAS5, see Johnson *et al.*<sup>31</sup>.

123 The rank histograms clearly indicate an under-forecasting bias of the absolute SON-3DP values  
124 within the UNSEEN ensemble (Supplementary Fig. 2). This is confirmed by the bootstrapping test,  
125 that shows that the observed mean and standard deviation fall outside the 95% confidence intervals  
126 of the UNSEEN ensemble (Supplementary Fig. 3). The UNSEEN SON-3DP anomalies and standardized  
127 anomalies do show rank uniformity, and thus are suggested to be reliable (Supplementary Fig. 2).  
128 Such under-forecasting biases precipitation extremes are not uncommon in global Earth System  
129 Models<sup>37</sup>, especially for a mountainous region like Western Norway.

130 As the UNSEEN SON-3DP deviations from the mean show good agreement to the observed values  
131 (Supplementary Fig. 2), the ratio between the mean observed extremes and the mean simulated  
132 extremes (1.74) is applied as a constant bias correction to generate the bias corrected UNSEEN  
133 ensemble (henceforth referred to as UNSEEN-BC). Note that we found little sensitivity to using the  
134 median (1.72), 5-year (1.69) or 20-year (1.70) values in the bias correction procedure and, hence  
135 chose a constant value to avoid extrapolations beyond the quantile range. The bootstrapping test  
136 shows that the statistics derived from the observed precipitation fall within the 95% intervals of  
137 UNSEEN-BC for timeseries of 35 years (Supplementary Fig. 4), i.e. the precipitation of the single  
138 realization of reality is one of the plausible realizations of UNSEEN-BC and, therefore, UNSEEN-BC is  
139 indistinguishable from the observed values.

140 We then fit the GEV distribution to the observations, the UNSEEN and the UNSEEN-BC ensemble (see  
141 Methods and Fig. 3). Interestingly, the fitted distributions show that the UNSEEN-BC ensemble  
142 diverges from the observed values for return periods above ~35 years. To evaluate the discrepancy,  
143 we test the sensitivity of the results to the choice of extreme value distribution (Supplementary Fig.  
144 5). Whilst the Gumbel distribution (shape parameter  $\xi = 0$ ) shows a relatively good fit to the  
145 observations and a similar distribution to the UNSEEN ensemble, the fit is not as good as using a full  
146 GEV with fitted shape parameter, as suggested by Supplementary Fig. 5 and confirmed by the  
147 likelihood ratio test ( $p$ -value = 0.03 for the observed and  $p$ -value =  $1.54 \cdot 10^{-7}$  for the UNSEEN  
148 ensemble). In addition, results are also very sensitive to outliers, as can be seen when the observed  
149 extreme value distribution is fitted on a sample where the largest value is increased by 10%  
150 (Supplementary Fig. 5). This confirms the challenge associated with estimating the magnitude of  
151 events of long return periods (greater than 20 years) from an observed time series of only 35 years,  
152 with more trust in estimations resulting from the larger UNSEEN sample.

153 We find that the 2005 and 2014 observed extreme events (two largest events in Fig. 3) are similar in  
154 magnitude and represent events with return periods of 21 years (CI of 19-24 years) when compared  
155 with the extreme value distribution of UNSEEN-BC. Based on the observed values, the return period  
156 estimate of 60 years for the events would be very uncertain, with the lower confidence interval  
157 never reaching the event magnitude (CI of 18 -  $\infty$  years). Moreover, the highest UNSEEN-BC event is  
158 1.5 times higher than the highest observed event, with an estimated return period of ~2000 years (CI  
159 of 1150-4800 years). The estimated return period of this event based on the observations is  
160 completely dominated by the uncertainties (~5000, 600 -  $\infty$  years) and can only be statistically  
161 modelled, while for the UNSEEN estimate, it is a physically simulated 'empirical' event within 3500  
162 years of data. The observed flood episode caused flooding and landslides with severe damage<sup>28</sup> and

163 UNSEEN-BC indicates what kind of events beyond the observed record are plausible in the present  
164 climate.

### 165 **UNSEEN-trends in 100-year precipitation over last 35 years**

166 Climate models can be used to detect changes<sup>38-41</sup> or to attribute extreme events to human causes<sup>42</sup>,  
167 but are less suited to detecting trends over the recent past such as the last 35 years. By design,  
168 climate model simulations are initialized once at the beginning of a centennial run. Contrastingly,  
169 here we use seasonal forecasts that are initialized every month, and thus are more constrained by  
170 real-world climate variability than climate model simulations. Consequently, seasonal forecasts  
171 sample a smaller range of climate conditions but are closer to reality than climate model  
172 simulations. This means that their use is consistent with analysing trends over the recent past  
173 described by the available forecast period (for SEAS5, currently 35 years). Furthermore, the model  
174 setup and version are the same for the entire hindcast simulation, ensuring that, with respect to the  
175 models and initialization, SEAS5 is a homogeneous dataset and thus suitable for climate analysis and  
176 detection of UNSEEN-trends.

177 With a 36 km resolution and 25 members, the ECMWF SEAS5 reforecast set used here is based on a  
178 modelling system of high resolution and associated with a large ensemble compared to current high-  
179 resolution global climate models<sup>43</sup>. SEAS5 greenhouse gas radiative forcing captures the long-term  
180 trends in emissions<sup>31</sup>, and we show that the global mean temperature trend in SEAS5 follows ERA5<sup>44</sup>  
181 (Supplementary Fig.6). Whilst regionally, we find a cold bias over the Norwegian study domain, the  
182 trend is consistent with ERA5 for both Western Norway and Svalbard (Supplementary Fig. 6),  
183 confirming the capacity of SEAS5 to detect recent trends.

184 To illustrate the added value of UNSEEN-trends, we extend the GEV distribution to include a time  
185 covariate and fit this distribution to the observed and UNSEEN SON-3DP (see Methods). Using the  
186 observations, we find an increase in 100-year SON-3DP of 4% over 1981-2015 in Western Norway,  
187 but associated with large uncertainties ranging from -27% to 34% (Fig. 4 a,b). The UNSEEN-trend  
188 estimate of 2% is more constrained due the larger sample size, with confidence intervals ranging  
189 from -3% to 7%. A negative trend is thus statistically possible, indicating that the trend over Western  
190 Norway is not significant. For Svalbard, we find a significant positive UNSEEN-trend of 8%, with  
191 uncertainty bounds ranging between 4-12%.

192 In addition to the trend in 100-year SON-3DP events, we illustrate the change in all return values by  
193 plotting the GEV distribution with the covariates 1981 and 2015 (Fig. 4 c,d). The likelihood ratio test  
194 shows that the GEV distribution including a time covariate improves the model fit for Svalbard (p-

195 value =  $2.7e-07$ ). We find that the frequency of the event that used to be a 100-year event in 1981  
196 has an expected return period of 41 years in 2015 (Fig. 4 c,d). For Western Norway, the GEV  
197 distribution including a time covariate does not improve the model fit for either the observed (p-  
198 value = 0.58) or the UNSEEN-ensemble (p-value = 0.65), and thus, the stationary GEV distribution, as  
199 presented in Fig. 3, is most appropriate.

## 200 **Discussion and Conclusion**

201 In this study, we test the robustness of the UNSEEN approach and we use the large sample to  
202 constrain short-term UNSEEN-trends in high-impact precipitation events for Western Norway and  
203 Svalbard. We show that with SEAS5, the effective sample size of autumn 3-day precipitation (SON-  
204 3DP) events in Western Norway and Svalbard can be increased by a factor of 100 compared to  
205 observations, because ensemble members are independent and the model is stable over lead times.  
206 Validating UNSEEN events and trends is a complex task, but our approach reproduces observed  
207 extremes well after bias correction for Western Norway, a region with extensive records<sup>26</sup>.

208 The insights presented in this study are specific to Western Norway and Svalbard SON-3DP but the  
209 independence, model stability and model fidelity tests applied to the UNSEEN approach could be  
210 transferred to other regions, temporal resolutions and spatial extent of the events, seasons and  
211 climate variables. Global validation of the UNSEEN ensemble will highlight in which regions the  
212 approach may enhance the robustness of design level estimation, with a potentially high value in  
213 supporting data scarce regions<sup>45</sup>. Furthermore, the large sample size may allow estimation of  
214 extremes using empirical approaches that avoid assumptions about underlying distributions and  
215 their non-stationarity, thereby offering the possibility of improved design estimates<sup>10</sup> and empirical  
216 attribution of physical mechanisms. A wide range of scientific disciplines might benefit from the  
217 UNSEEN method by forcing seasonal prediction systems into impact models to assess  
218 unprecedented impacts and improve understanding of the physical mechanisms leading to these  
219 events.

220 The results from the two study areas highlight the value of both the UNSEEN and the UNSEEN-trends  
221 approach. For the well-monitored Norwegian domain, we are able to bias correct the UNSEEN  
222 ensemble (UNSEEN-BC) and therefore we can better estimate the return period of the 2005 and  
223 2014 flood episodes. We find that the flood episodes are not rare exceptions; rather they might be  
224 expected to occur once in 20 years under a stationary climate. Furthermore, the UNSEEN-BC  
225 ensemble shows that an event of 1.5 times the magnitude of the highest observed event could arise.  
226 The September 2005 and October 2014 flood episodes were identified as high-impact events in  
227 previous end-user engagement sessions within the Translating Weather Extremes into the Future

228 (TWEX) project, and thus, the results found from the UNSEEN-BC ensemble are of high relevance to  
229 decision makers and end-users. This application of the UNSEEN approach is similar to previous  
230 research on the 2013/14 winter floods in the UK<sup>22</sup> and for the 1990 windstorm losses over Germany  
231 and the UK<sup>19</sup>. A difference to the previous studies is that we run the analysis on a three-day  
232 resolution, whereas monthly averages have been used so far. The observed record and the UNSEEN-  
233 trend show that there is no significant trend over Western Norway between 1981-2015, and  
234 therefore justify using the stationary GEV distribution.

235 Contrastingly, for Svalbard, the UNSEEN-trends approach shows that what was a 100-year event in  
236 1981 is to be expected to return once in 41 years in 2015. The trend in extreme precipitation over  
237 Svalbard could not be detected from observation-based studies due to the sparse observation  
238 network in this area<sup>27</sup>. Despite very few precipitation extremes being recorded in the Svalbard  
239 Archipelago, it is assumed that their frequency and magnitude are increasing in a warming  
240 climate<sup>27,30,46</sup>, which is confirmed by our UNSEEN-trends analysis. Those precipitation extremes are  
241 connected to the inflow of relatively warm air and, thus, can cause severe landslides and so-called  
242 rain-on-ice events<sup>30</sup>. Both could have significant impacts on people living in the Arctic and on the  
243 local ecosystem.

244 In due course, the drivers of changes in climate extremes could be investigated with the UNSEEN-  
245 trends approach. For example, to assess the non-stationarity of extreme precipitation, covariates  
246 other than time could be selected, such as ocean temperatures, modes of climate variability, or  
247 indicators of large-scale synoptic weather systems. This may improve our physical understanding of  
248 the non-stationary processes and could provide insight into potential model biases, thereby  
249 improving confidence in detected trends. Century-long seasonal hindcasts, such as the ASF-20C  
250 global atmospheric seasonal hindcasts<sup>47</sup>, might prove useful in assessing the sensitivity of UNSEEN-  
251 trends to different time windows over a longer time period.

252 Our results for Western Norway highlight the strength of UNSEEN in estimating design-levels and  
253 present-day climate hazards, backed by a growing body of literature<sup>12,13,22,14-21</sup>, and the results for  
254 Svalbard emphasise the significance of our novel UNSEEN-trends approach in estimating non-  
255 stationarities in climate extremes. Both underline the need to rethink current design-level estimates  
256 based upon observations alone. We think further applications can 1) help estimate design values,  
257 especially relevant for data scarce regions; 2) improve risk estimation of natural hazards by coupling  
258 UNSEEN to impact models; 3) detect trends in rare climate extremes, including variables other than  
259 precipitation; and 4) increase our physical understanding of the drivers of non-stationary climate  
260 extremes, through the possible attribution of detected trends.



262 **References**

- 263 1. IPCC. Summary for Policymakers. in *Global Warming of 1.5°C. An IPCC Special Report on the*  
 264 *impacts of global warming of 1.5°C above pre-industrial levels and related global greenhouse*  
 265 *gas emission pathways, in the context of strengthening the global response to the threat of*  
 266 *climate change*, 32 (World Meteorological Organization, 2018).
- 267 2. IPCC. Summary for Policymakers. in *Managing the Risks of Extreme Events and Disasters to*  
 268 *Advance Climate Change Adaptation: Special Report of the Intergovernmental Panel on*  
 269 *Climate Change 3–22* (Cambridge University Press, 2012).  
 270 doi:10.1017/CBO9781139177245.003.
- 271 3. IPCC. Summary for Policymakers. in *Climate Change 2014: Impacts, Adaptation, and*  
 272 *Vulnerability. Part A: Global and Sectoral Aspects. Contribution of Working Group II to the*  
 273 *Fifth Assessment Report of the Intergovernmental Panel on Climate Change 1–32* (Cambridge  
 274 University Press, 2014). doi:10.1017/CBO9781107415379.003.
- 275 4. Wilby, R. L. *et al.* The ‘dirty dozen’ of freshwater science: detecting then reconciling  
 276 hydrological data biases and errors. *Wiley Interdiscip. Rev. Water* **4**, e1209 (2017).
- 277 5. Zwiers, F. W. *et al.* Climate Extremes: Challenges in Estimating and Understanding Recent  
 278 Changes in the Frequency and Intensity of Extreme Climate and Weather Events. in *Climate*  
 279 *Science for Serving Society* 339–389 (Springer Netherlands, 2013). doi:10.1007/978-94-007-  
 280 6692-1\_13.
- 281 6. Alexander, L. V. Global observed long-term changes in temperature and precipitation  
 282 extremes: a review of progress and limitations in IPCC assessments and beyond. *Weather*  
 283 *Clim. Extrem.* **11**, 4–16 (2016).
- 284 7. Klein Tank, A. M. G. & Können, G. P. Trends in Indices of Daily Temperature and Precipitation  
 285 Extremes in Europe, 1946–99. *J. Clim.* **16**, 3665–3680 (2003).
- 286 8. Westra, S., Alexander, L. V & Zwiers, F. W. Global increasing trends in annual maximum daily  
 287 precipitation. *J. Clim.* **26**, 3904–3918 (2013).
- 288 9. Donat, M. G., Lowry, A. L., Alexander, L. V, O’Gorman, P. A. & Maher, N. More extreme  
 289 precipitation in the world’s dry and wet regions. *Nat. Clim. Chang.* **6**, 508 (2016).
- 290 10. der Wiel, K., Wanders, N., Selten, F. M. & Bierkens, M. F. P. Added Value of Large Ensemble  
 291 Simulations for Assessing Extreme River Discharge in a 2 °C Warmer World. *Geophys. Res.*  
 292 *Lett.* **46**, (2019).
- 293 11. Berghuijs, W. R., Aalbers, E. E., Larsen, J. R., Trancoso, R. & Woods, R. A. Recent changes in  
 294 extreme floods across multiple continents. *Environ. Res. Lett.* **12**, 114035 (2017).
- 295 12. van den Brink, H. W., Können, G. P., Opsteegh, J. D., van Oldenborgh, G. J. & Burgers, G.  
 296 Improving 10<sup>4</sup>-year surge level estimates using data of the ECMWF seasonal prediction  
 297 system. *Geophys. Res. Lett.* **31**, L17210 (2004).
- 298 13. van den Brink, H. W., Können, G. P., Opsteegh, J. D., van Oldenborgh, G. J. & Burgers, G.  
 299 Estimating return periods of extreme events from ECMWF seasonal forecast ensembles. *Int.*  
 300 *J. Climatol.* **25**, 1345–1354 (2005).
- 301 14. Kent, C. *et al.* Maize Drought Hazard in the Northeast Farming Region of China:  
 302 Unprecedented Events in the Current Climate. *J. Appl. Meteorol. Climatol.* **58**, 2247–2258

- 303 (2019).
- 304 15. Breivik, Ø., Aarnes, O. J., Abadalla, S., Bidlot, J.-R. & Janssen, P. Wind and Wave Extremes over  
305 the World Oceans From Very Large Ensembles. *Geophys. Res. Lett.* **41**, 5122–5131 (2014).
- 306 16. Breivik, Ø., Aarnes, O. J., Bidlot, J.-R., Carrasco, A. & Saetra, Ø. Wave Extremes in the  
307 Northeast Atlantic from Ensemble Forecasts. *J. Clim.* **26**, 7525–7540 (2013).
- 308 17. Osinski, R. *et al.* An approach to build an event set of European windstorms based on  
309 ECMWF EPS. *Nat. Hazards Earth Syst. Sci.* **16**, 255–268 (2016).
- 310 18. Meucci, A., Young, I. R. & Breivik, Ø. Wind and Wave Extremes from Atmosphere and Wave  
311 Model Ensembles. *J. Clim.* **31**, 8819–8842 (2018).
- 312 19. Walz, M. A. & Leckebusch, G. C. Loss potentials based on an ensemble forecast: How likely  
313 are winter windstorm losses similar to 1990? *Atmos. Sci. Lett.* **20**, e891 (2019).
- 314 20. Thompson, V. *et al.* Risk and dynamics of unprecedented hot months in South East China.  
315 *Clim. Dyn.* **52**, 2585–2596 (2019).
- 316 21. Kent, C. *et al.* Using climate model simulations to assess the current climate risk to maize  
317 production. *Environ. Res. Lett.* **12**, (2017).
- 318 22. Thompson, V. *et al.* High risk of unprecedented UK rainfall in the current climate. *Nat.*  
319 *Commun.* **8**, 107 (2017).
- 320 23. Shepherd, T. G. *et al.* Storylines: an alternative approach to representing uncertainty in  
321 physical aspects of climate change. *Clim. Change* **151**, 555–571 (2018).
- 322 24. Lavers, D. A. & Villarini, G. The contribution of atmospheric rivers to precipitation in Europe  
323 and the United States. *J. Hydrol.* **522**, 382–390 (2015).
- 324 25. Lussana, C. *et al.* seNorge2 daily precipitation, an observational gridded dataset over Norway  
325 from 1957 to the present day. *Earth Syst. Sci. Data* **10**, 235–249 (2018).
- 326 26. Lussana, C., Tveito, O. E., Dobler, A. & Tunheim, K. seNorge\_2018, daily precipitation and  
327 temperature datasets over Norway. *Earth Syst. Sci. Data Discuss.* **2019**, 1–27 (2019).
- 328 27. Serreze, M. C., Crawford, A. D. & Barrett, A. P. Extreme daily precipitation events at  
329 Spitsbergen, an Arctic Island. *Int. J. Climatol.* **35**, 4574–4588 (2015).
- 330 28. Stohl, A., Forster, C. & Sodemann, H. Remote sources of water vapor forming precipitation on  
331 the Norwegian west coast at 60°N - A tale of hurricanes and an atmospheric river. *J. Geophys.*  
332 *Res. Atmos.* **113**, (2008).
- 333 29. Langsholt, E., Roald, L. A., Holmqvist, E. & Fleig, A. *Flommen på Vestlandet oktober 2014. NVE*  
334 *Report* www.nve.no (2015).
- 335 30. Hansen, B. B. *et al.* Warmer and wetter winters: characteristics and implications of an  
336 extreme weather event in the High Arctic. *Environ. Res. Lett.* **9**, 114021 (2014).
- 337 31. Johnson, S. J. *et al.* SEAS5: The new ECMWF seasonal forecast system. *Geosci. Model Dev.*  
338 *Discuss.* (2018) doi:<https://doi.org/10.5194/gmd-12-1087-2019>.
- 339 32. Lavers, D. A., Pappenberger, F. & Zsoter, E. Extending medium-range predictability of extreme  
340 hydrological events in Europe. *Nat. Commun.* **5**, 5382 (2014).
- 341 33. Baggett, C. F., Barnes, E. A., Maloney, E. D. & Mundhenk, B. D. Advancing atmospheric river  
342 forecasts into subseasonal-to-seasonal time scales. *Geophys. Res. Lett.* **44**, 7528–7536 (2017).

- 343 34. Gupta, A. Sen, Jourdain, N. C., Brown, J. N. & Monselesan, D. Climate drift in the CMIP5  
344 models. *J. Clim.* **26**, 8597–8615 (2013).
- 345 35. Hermanson, L. *et al.* Different types of drifts in two seasonal forecast systems and their  
346 dependence on ENSO. *Clim. Dyn.* **51**, 1411–1426 (2018).
- 347 36. Wilks, D. S. *Statistical methods in the atmospheric sciences*. vol. 100 (Academic press, 2011).
- 348 37. Sillmann, J., Kharin, V. V., Zhang, X., Zwiers, F. W. & Bronaugh, D. Climate extremes indices in  
349 the CMIP5 multimodel ensemble: Part 1. Model evaluation in the present climate. *J. Geophys.*  
350 *Res. Atmos.* **118**, 1716–1733 (2013).
- 351 38. Kharin, V. V *et al.* Risks from climate extremes change differently from 1.5 °C to 2.0 °C  
352 depending on rarity. *Earth's Futur.* (2018) doi:<https://doi.org/10.1002/2018EF000813>.
- 353 39. Kharin, V. V, Zwiers, F. W., Zhang, X. & Wehner, M. Changes in temperature and precipitation  
354 extremes in the CMIP5 ensemble. *Clim. Change* **119**, 345–357 (2013).
- 355 40. Sillmann, J., Kharin, V. V, Zwiers, F. W., Zhang, X. & Bronaugh, D. Climate extremes indices in  
356 the CMIP5 multimodel ensemble: Part 2. Future climate projections. *J. Geophys. Res. Atmos.*  
357 **118**, 2473–2493 (2013).
- 358 41. Kharin, V. V & Zwiers, F. W. Changes in the extremes in an ensemble of transient climate  
359 simulations with a coupled atmosphere--ocean GCM. *J. Clim.* **13**, 3760–3788 (2000).
- 360 42. Angéilil, O. *et al.* Comparing regional precipitation and temperature extremes in climate  
361 model and reanalysis products. *Weather Clim. Extrem.* **13**, 35–43 (2016).
- 362 43. Haarsma, R. J. *et al.* High Resolution Model Intercomparison Project (HighResMIP v1.0) for  
363 CMIP6. *Geosci. Model Dev.* **9**, 4185–4208 (2016).
- 364 44. Hersbach, H. *et al.* *Operational global reanalysis: progress, future directions and synergies*  
365 *with NWP including updates on the ERA5 production status. ERA Report Series No. 27* (2018)  
366 doi:10.21957/tkic6g3wm.
- 367 45. Courty, L. G., Wilby, R. L., Hillier, J. K. & Slater, L. J. Intensity-duration-frequency curves at the  
368 global scale. *Environ. Res. Lett.* **14**, (2019).
- 369 46. Hanssen-Bauer, I. *et al.* *Climate in Svalbard 2100*. (2019).
- 370 47. Weisheimer, A., Schaller, N., O'Reilly, C., MacLeod, D. A. & Palmer, T. Atmospheric seasonal  
371 forecasts of the twentieth century: multi-decadal variability in predictive skill of the winter  
372 North Atlantic Oscillation (NAO) and their potential value for extreme event attribution. *Q. J. R.*  
373 *Meteorol. Soc.* **143**, 917–926 (2017).
- 374 48. Madec, G. & others. NEMO ocean engine. *Note du Pôle modélisation l'Institut Pierre-Simon*  
375 *Laplace No 27* ISSN No 1288-1619 (2016).
- 376 49. Fichefet, T. & Maqueda, M. A. Sensitivity of a global sea ice model to the treatment of ice  
377 thermodynamics and dynamics. *J. Geophys. Res. Ocean.* **102**, 12609–12646 (1997).
- 378 50. Dee, D. P. *et al.* The ERA-Interim reanalysis: Configuration and performance of the data  
379 assimilation system. *Q. J. R. Meteorol. Soc.* **137**, 553–597 (2011).
- 380 51. Zuo, H., Alonso-Balmaseda, M. A., Mogensen, K. & Tietsche, S. OCEAN5: The ECMWF Ocean  
381 Reanalysis System and its Real-Time analysis component. *ECMWF Tech. Memo.* (2018)  
382 doi:<https://doi.org/10.21957/la2v0442>.
- 383 52. Azad, R. & Sorteberg, A. Extreme daily precipitation in coastal western Norway and the link to

- 384 atmospheric rivers. *J. Geophys. Res. Atmos.* **122**, 2080–2095 (2017).
- 385 53. Benedict, I., Ødemark, K., Nipen, T. & Moore, R. Large-scale flow patterns associated with  
386 extreme precipitation and atmospheric rivers over Norway. *Mon. Weather Rev.* **147**, 1415–  
387 1428 (2019).
- 388 54. Zhang, X. *et al.* Indices for monitoring changes in extremes based on daily temperature and  
389 precipitation data. *Wiley Interdiscip. Rev. Clim. Chang.* **2**, 851–870 (2011).
- 390 55. Hoyer, S. & Hamman, J. J. xarray: N-D labeled Arrays and Datasets in Python. *J. Open Res.*  
391 *Softw.* **5**, (2017).
- 392 56. Gómez-Rubio, V. ggplot2 - Elegant Graphics for Data Analysis (2nd Edition). *J. Stat. Softw.* **77**,  
393 (2017).
- 394 57. Press, S. J. *Applied multivariate analysis: using Bayesian and frequentist methods of inference.*  
395 (Courier Corporation, 2005).
- 396 58. R Core Team. R: A Language and Environment for Statistical Computing. [https://www.R-](https://www.R-project.org)  
397 [project.org](https://www.R-project.org) (2019).
- 398 59. Hyndman, R. J. & Fan, Y. Sample Quantiles in Statistical Packages. *Am. Stat.* **50**, 361–365  
399 (1996).
- 400 60. Coles, S., Bawa, J., Trenner, L. & Dorazio, P. *An introduction to statistical modeling of extreme*  
401 *values.* vol. 208 (Springer, 2001).
- 402 61. Gilleland, E., Katz, R. W. & others. extRemes 2.0: an extreme value analysis package in R. *J.*  
403 *Stat. Softw.* **72**, 1–39 (2016).
- 404 62. Katz, R. W., Parlange, M. B. & Naveau, P. Statistics of extremes in hydrology. *Adv. Water*  
405 *Resour.* **25**, 1287–1304 (2002).
- 406 63. Katz, R. W. Statistical methods for nonstationary extremes. in *Extremes in a Changing Climate*  
407 15–37 (Springer, 2013).
- 408 64. Rojas, R., Feyen, L. & Watkiss, P. Climate change and river floods in the European Union:  
409 Socio-economic consequences and the costs and benefits of adaptation. *Glob. Environ.*  
410 *Chang.* **23**, 1737–1751 (2013).

411

## 412 **Methods**

413 **Data.** We use the fifth generation of the ECMWF seasonal forecasting system SEAS5 to generate the  
414 UNSEEN ensemble. SEAS5 is a global coupled ocean, sea-ice, and atmosphere model, which has been  
415 introduced in fall 2017<sup>31</sup>. The atmospheric component is based on cycle 43r1 of the ECMWF  
416 Integrated Forecast System. The spatial horizontal resolution is 36 km and it has 91 vertical levels.  
417 The ocean (Nucleus for European Modelling of the Ocean, NEMO<sup>48</sup>) and sea-ice (Louvain-la-Neuve  
418 Sea Ice Model, LIM2<sup>49</sup>) models run on a 0.25-degree resolution. The atmosphere is initialized by ERA-  
419 Interim<sup>50</sup> and the ocean and sea-ice components are initialized by the OCEAN5 reanalysis<sup>51</sup>. ECMWF  
420 provides a re-forecast (also known as hindcast) dataset for calibration of the operational forecasting  
421 system SEAS5. The data are initialized monthly with 25 ensemble members, each with 7-month

422 forecast length on a daily resolution, covering the years 1981-2016<sup>31</sup>. The ensemble members are  
423 generated from perturbations to the ocean and atmosphere initial conditions and from stochastic  
424 model perturbations.

425

426 In the UNSEEN approach, ensemble members and initialization dates are pooled to increase the  
427 sample size of the variable of interest. Here, we generate an UNSEEN ensemble for the west coast of  
428 Norway and for the Svalbard Archipelago to focus on recent atmospheric river (AR) related severe  
429 events<sup>27-29</sup>. ARs have been connected to precipitation extremes in the observed records for both  
430 Norway<sup>52,53</sup> and Svalbard<sup>27</sup> and occur in September to March. AR-related floods mostly occur in  
431 autumn, because snowfall during winter precipitation events results in storage rather than runoff.  
432 One-day and five-day precipitation are a common diagnostic for extreme analysis<sup>6,54</sup>. ARs frequently  
433 strengthen over a period of several days<sup>28,29</sup> and therefore multi-day diagnostics prevent splitting  
434 events. Following the 2014 flood episode<sup>29</sup>, we have chosen three-day total precipitation in this  
435 study. We thus select autumn (September to November) 3-day extreme precipitation (SON-3DP) as  
436 target events.

437

438 Since the forecasts are initialized every month on the first of the month and run over 7-months  
439 length, there are five initialization months (May-September) available to forecast the entire target  
440 autumn season (September-November). The first month is removed to avoid potentially dependent  
441 events. In the end, 100 forecasts, based on 25 ensemble members with 4 initialization dates are  
442 used to forecast the autumn season of each year (Fig. 1a-c). The window of 35 years between 1981  
443 and 2016 leads to a total of 3500 forecasts of autumn weather conditions that could have occurred.  
444 We extract the maximum 3-day cumulative precipitation within autumn from the 3500 forecasts  
445 (SON-3DP), using the xarray package<sup>55</sup> in Python. To focus on the large-scale systems as experienced  
446 in recent severe events, we use only the large-scale precipitation output of the model. The west  
447 coast of Norway is mountainous and characterised by large topographic variations. Catchment-scale  
448 processes in these mountainous areas cannot be resolved by a global model with 36 km resolution.  
449 Therefore, the precipitation timeseries presented in this study are spatial averages where the 200-  
450 year precipitation exceeds 90 mm for the west coast of Norway (4-7° E, 58-63° N) and 35 mm for  
451 Svalbard (8-30° E, 76-80° N) (Supplementary Fig. 1).

452

453 To evaluate the precipitation extremes simulated by SEAS5, we use a 1x1 km gridded station-based  
454 precipitation product for Norway<sup>25</sup>. The data have recently been corrected for underestimation  
455 caused by wind-induced under catch and uses more information in the interpolation scheme for

456 data-scarce areas, resulting in higher precipitation in data scarce areas<sup>26</sup>. We upscale this gridded  
457 dataset to the same resolution as SEAS5 and extract SON-3DP values for the same spatial domain  
458 over 1981-2016. Note, for the Svalbard Archipelago no gridded precipitation dataset is available as a  
459 reference dataset. We use ERA5<sup>44</sup> for the global and regional temperature evaluation of SEAS5.

460

461 **Ensemble member independence testing.** The method for independence testing applied in this  
462 study is inspired by previous research on potential predictability: the ability of the model to predict  
463 itself<sup>32,36</sup>. The potential predictability of a model is calculated by using one of the forecast ensemble  
464 members as the observations and the mean of the other ensemble members as the forecast. The  
465 correlation between the 'observed' ensemble member and the mean of the other ensemble  
466 members is calculated for every ensemble member and this range gives an estimate of the ability of  
467 the model to forecast itself. Because this method assesses the correlation between ensemble  
468 members, it can be used to find the degree of ensemble members' dependence. In seasonal  
469 forecasting, this method is used to identify any predictability in the seasonal prediction system. In  
470 contrast, here we seek to demonstrate that there is no potential predictability in the system for the  
471 ensemble members to represent independent, unique events.

472 An illustration of our method to test for independence is shown in Fig. 1. A potential predictability  
473 test is performed but instead of correlating an ensemble member to the mean of the other  
474 ensemble members, a pairwise correlation test is applied between all ensemble members to  
475 robustly assess the individual ensemble member dependence. Indeed, we concatenate the seasons  
476 together member by member, even though they do not necessarily originate from the same run.  
477 This approach was chosen because the underlying initialization method remains the same for each  
478 member over different seasons.

479 For the 25 ensemble members, there are 300 distinct pairings in the correlation matrix for each of  
480 the four lead times being analysed (may-August). We calculate the spearman  $\rho$  statistics on the  
481 standardized SON-3DP anomalies (deviation from mean divided by the standard deviation) for each  
482 distinct pair. From the 300  $\rho$  values for each lead time, boxplot statistics are calculated: the  
483 whiskers, the interquartile range and the median. When testing for significance of the 300  $\rho$  values,  
484 care must be taken not to falsely detect significant correlations because of the large number of tests.  
485 For example, with a confidence interval of 5%, 15 out of the 300 correlations would be expected to  
486 be significant by chance alone. To avoid these problems, a permutation test is performed. The  
487 dataset, which previously consisted of 25 timeseries (members) of 35 datapoints (years) for four  
488 initializations months (lead times), is resampled into 100 timeseries of 35 datapoints, with

489 datapoints randomly picked from all members, years and lead times to remove potential  
 490 correlations. This randomized dataset is split into four pseudo lead times of 25 timeseries, in order  
 491 to calculate the boxplot statistics from the same amount of correlation coefficients (300) as before.  
 492 The data are resampled 1000 times (without replacement), resulting in 4000 boxplot statistics (4  
 493 pseudo lead times \* 1000 resampled series), from which the confidence intervals are calculated  
 494 based on a 5% significance level (the 2.5 and 97.5 percentiles).

495

496 **Model stability.** The extreme precipitation distribution must be similar over lead times in order to  
 497 generate the UNSEEN ensemble. We use four initialization months (May-August) forecasting the  
 498 target autumn season with lead times 2-5 months. For each lead time, 25 ensemble members over  
 499 35 years result into an 875-year long dataset and the pooled ensemble into 3500 years. To compare  
 500 the distributions, we first plot the probability density function for each of the lead times using  
 501 ggplot2<sup>56</sup>. Secondly, we plot the extreme value distributions, focussing more on the tails of the  
 502 distribution. We calculate empirical quantiles of the extreme precipitation ensemble without  
 503 assuming any distribution a priori, to avoid problems regarding statistical modelling of the  
 504 extremes<sup>10,57</sup>. The quantile ( $Q$ ) of a distribution is the inverse of the distribution function ( $F(x)$ ):

$$505 \quad Q(p) = F^{-1}(p) = \inf \{x: F(x) \geq p\}, \quad 0 < p < 1 \quad (1)$$

506 Where the return value is associated with the quantile of percentile ( $p$ ):

$$507 \quad p = 1 - \frac{1}{T} \quad (2)$$

508 With  $T$  being the return period. We use the quantile function in  $R$ <sup>58</sup> to compute the empirical return  
 509 values and we refer to Hyndman & Fan<sup>59</sup> for more specifics.

510

511 **Fidelity of the UNSEEN ensemble for Western Norway.** We first evaluate the UNSEEN ensemble and  
 512 then compare UNSEEN design-levels to observation-based design-levels. As a first assessment of the  
 513 biases within the SON-3DP UNSEEN ensemble, we use rank histograms. Rank histograms indicate  
 514 over-dispersion or under-dispersion and over-forecasting or under-forecasting bias<sup>36</sup>. Here, we have  
 515 100 members (4 lead times and 25 ensemble members) for each year over 1981-2015. The rank of  
 516 the observations within the 100 ensembles is calculated for each year and the resulting 35 ranks are  
 517 plotted as a histogram over the range 1-100. If the observations are mostly in the upper (lower)  
 518 ranks, this indicates that the observed values are higher (lower) than the forecasted values and  
 519 therefore the forecasts are under-forecasting (over-forecasting). Similarly, when the observations

520 are mostly in the outer (inner) ranks, this indicates that the observed values show more (less)  
 521 variability and thus the forecasts are under-dispersed (over-dispersed). We create rank histograms  
 522 for the raw SON-3DP UNSEEN ensemble, for the anomalies from the mean and for the standardized  
 523 anomalies, where the anomalies are divided by the standard deviation.

524 To compare UNSEEN to the observed record in more detail, we apply a bootstrap test presented in  
 525 previous studies<sup>20,22</sup>. We bootstrap 10,000 timeseries of 35 years with replacement from all  
 526 ensembles (100 x 35 years) and calculate the mean, standard deviation, skewness and kurtosis for  
 527 each. We test whether the four distribution statistics derived from the observed precipitation time  
 528 series over the period 1981-2015 fall within the 95% confidence intervals for the statistics derived  
 529 from the bootstrapped timeseries.

530 We then fit the Generalized Extreme Value (GEV) distribution, described by a location ( $-\infty < \mu <$   
 531  $\infty$ ), scale ( $\sigma > 0$ ) and shape ( $-\infty < \xi < \infty$ ) parameter<sup>60</sup>:

$$532 \quad F(x) = \exp \left[ - \left( 1 + \xi \left( \frac{x-\mu}{\sigma} \right) \right)^{-\frac{1}{\xi}} \right], \quad \left( 1 + \xi \left( \frac{x-\mu}{\sigma} \right) \right) > 0 \quad (3)$$

533 And we test the sensitivity to using the Gumbel distribution with  $\xi = 0$ , simplifying the distribution  
 534 to:

$$535 \quad F(x) = \exp \left[ - \exp \left( - \left( \frac{x-\mu}{\sigma} \right) \right) \right], \quad -\infty < x < \infty \quad (4)$$

536 The quantiles of the distribution can again be obtained by inverting the distribution:

$$537 \quad x_p = \begin{cases} \mu - \frac{\sigma}{\xi} [1 - \{-\log(1-p)\}^{-\xi}], & \text{for } \xi \neq 0 \\ \mu - \sigma \log\{-\log(1-p)\} & , \quad \text{for } \xi = 0 \end{cases} \quad (5)$$

538 Where the return value  $x_p$  corresponds to the return period 1/probability ( $p$ ). For all statistical  
 539 model fits in this study (including non-stationary fits described in the next section), we apply  
 540 Maximum Likelihood Estimation (MLE) to estimate the parameters of the distributions, utilizing the  
 541 extRemes package<sup>61</sup> in R<sup>58</sup>. The 95% confidence intervals of the distributions are calculated based on  
 542 the normal approximation, which is the default of the extRemes package.

543

544 **UNSEEN-trends.** In this study, we present the idea of performing trend analysis on seasonal  
 545 hindcast, as the seasonal hindcasts provide a larger sample than observations and a higher  
 546 resolution than climate models (see the UNSEEN-trends section for more details). We apply well-  
 547 established extreme value theory<sup>60,62,63</sup>, by allowing the location ( $\mu$ ) and scale ( $\sigma$ ) parameters of the



548 GEV distribution (given in equation 3) to vary linearly with time ( $t$ ). Because the scale parameter  
549 needs to be positive, a log-link function is used:

$$550 \quad \mu(t) = \mu_0 + \mu_1 t \quad (6)$$

$$551 \quad \ln \sigma(t) = \phi_0 + \phi_1 t \quad (7)$$

552

553 This approach selects one block maximum per year, leading to 35 data points over the years 1981-  
554 2015 based on observed records. With UNSEEN-trends, we have 100 times more values for each  
555 year and thus increase confidence in the regression analysis (see Fig.4a,b for illustration). As for the  
556 stationary method, we use MLE to estimate the parameters of the distributions and the normal  
557 approximation to find the 95% confidence intervals of return values. We focus on the changes in the  
558 100-year quantiles, because these are associated with the design-levels mostly used in flood  
559 defence<sup>64</sup>. The trend in the 100-year return value is defined as the percentual change between 1981  
560 and 2015:

$$561 \quad \Delta x_T = 100 * \left( \frac{x_T(\mu_{2015}, \ln \sigma_{2015}, \xi) - x_T(\mu_{1981}, \ln \sigma_{1981}, \xi)}{x_T(\mu_{1981}, \ln \sigma_{1981}, \xi)} \right)$$

562 Where  $x_T$  is defined by equation (5).

563 The robustness of the trends to experiment decisions like the block size and the regression method  
564 can be further investigated but are beyond the scope of this research. For example, 6-month blocks  
565 can be selected at the expense of the ensemble size. This will result in 25 realizations, in comparison  
566 with 3-month blocks, which contain 100 realizations. A block size of three months (September-  
567 November) is chosen in this study. A linear trend in time is assumed in this study. With the large  
568 amount of data, more complex regression methods can be explored. The ECMWF SEAS5 seasonal  
569 prediction system is used in this study, but other seasonal prediction systems with available  
570 hindcasts could also be assessed to test the model sensitivity to return value and trend estimation.

## 571 **Acknowledgements**

572 We acknowledge A.V. Dyrddal, J. Sillmann and A. Weisheimer for their input that helped improve the  
573 paper. TK acknowledges support from NERC CENTA Doctoral Training Partnership and funding from  
574 both the Norwegian Meteorological Institute and Loughborough University. MM acknowledge  
575 funding from the TWEX project (grant 255037).

## 576 **Data and code availability**

577 SEAS5 re-forecast data and ERA-5 data are openly available on the Copernicus Climate Change  
578 Service (C3S) Climate DataStore (<https://cds.climate.copernicus.eu/>) and the SeNorge daily total  
579 precipitation data are available at DOI: <https://doi.org/10.5281/zenodo.2082320>. The extracted  
580 SON-3DP UNSEEN ensembles as well as the extracted SON-3DP observations will be made available  
581 on GitHub, along with all code to reproduce the analysis in this paper. Code is available to reviewers  
582 on request.

### 583 **Author contributions**

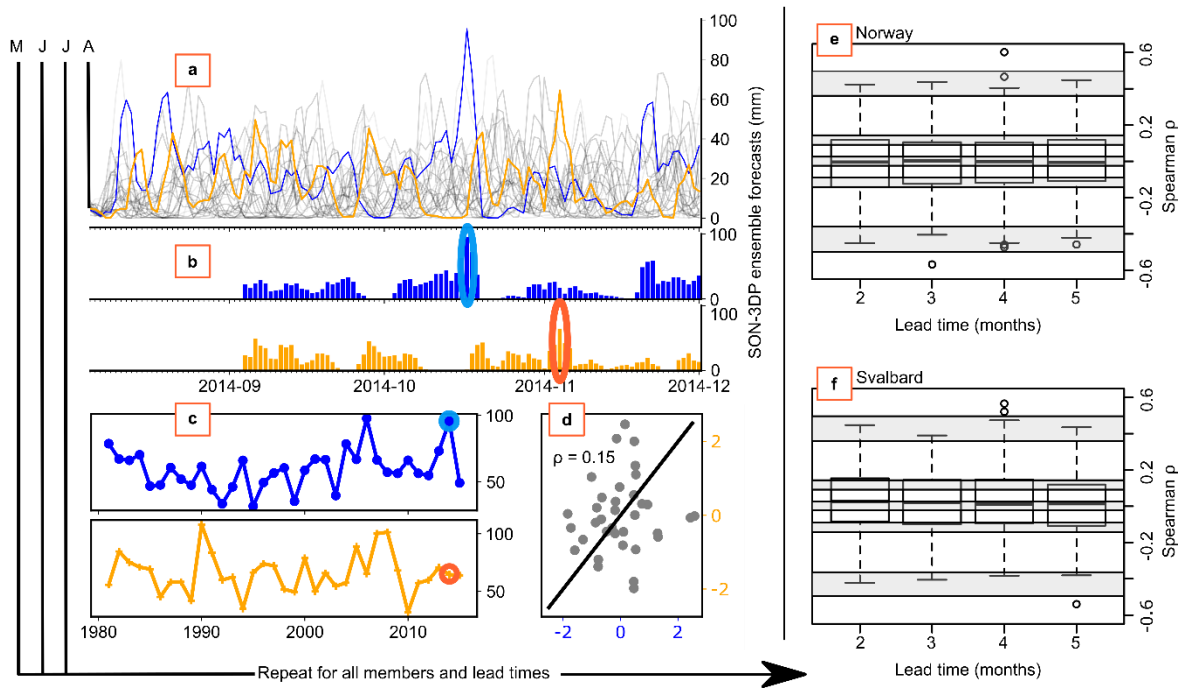
584 T.K. and M.M. conceived and T.K, M.M, L.J.S., T.M., R.L.W., C.P., P.B. designed the study. T.K. drafted  
585 the paper with extensive contributions from L.J.S., T.M., R.L.W., C.P. and M.M.. T.K. analysed the  
586 data with input from all authors. M.M. acquired the data. T.K. produced the figures; L.F. produced  
587 Supplementary Fig. 6.

### 588 **Competing interests**

589 The authors declare no competing interests.

590

591 **Figures**



592

593 **Fig. 1 | A workflow for analysing ensemble member dependence.** **a**, August 2014 initialized 25-  
 594 member seasonal forecasts of 3-day precipitation time series over the SON forecast horizon.  
 595 Ensemble members 0 and 1 are shown in blue and orange, respectively. **b**, From the forecast  
 596 members 0 and 1, the September-November (SON) maximum value for the 2014 season is selected.  
 597 **c**, A series of the maximum 3-day precipitation values for the SON season for each year in the  
 598 hindcast record is created for member 0 and member 1. The 2014 maximum, as illustrated in **b**, is  
 599 encircled. **d**, The standardized anomaly of the maximum 3-day precipitation series for the two  
 600 members are correlated. Spearman's  $\rho$  correlation is shown. This process is repeated for the 300  
 601 distinct ensemble member pairings for each of the four lead times (May-August). **e,f**, Boxplots of the  
 602 resulting 300 Spearman's  $\rho$  correlations for each lead time over Norway (**e**) and Svalbard (**f**). Grey  
 603 shading shows the confidence intervals of the boxplot statistics (whiskers, interquartile range and  
 604 median), based on a permutation test with 5% significance level.

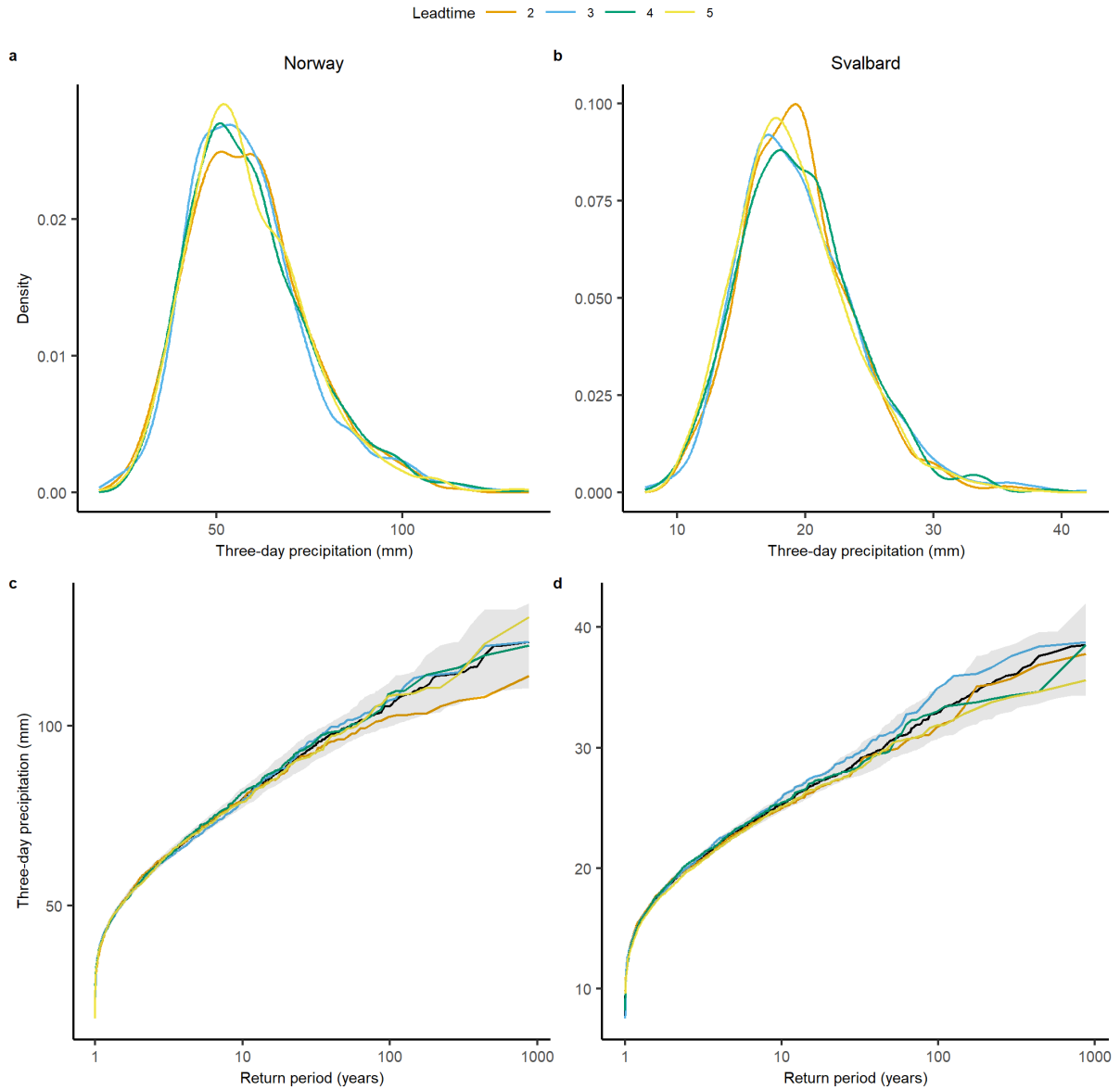
605

606

607

608

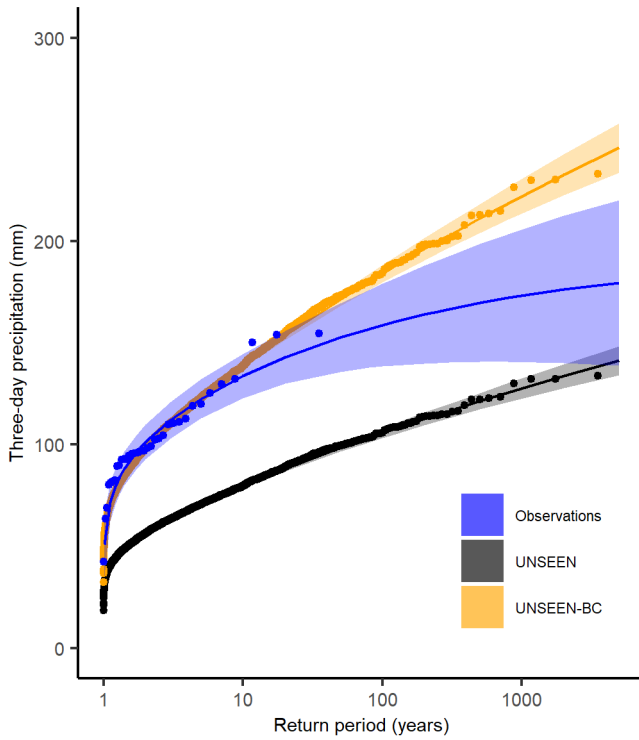
609



610

611 **Fig. 2 | SEAS5 model stability of extreme precipitation over Western Norway and Svalbard.** The  
 612 empirical probability density (**a,b**) and extreme value (**c,d**) distribution of SON-3DP for each lead time  
 613 and for all lead times together (in black), for the West Coast (**a,c**) and Svalbard (**b,d**) domains. Grey  
 614 shading in **c,d**, illustrates the 95% confidence intervals of the distribution of the pooled lead times,  
 615 bootstrapped to timeseries of similar length to the individual lead times with  $n = 10,000$ .

616



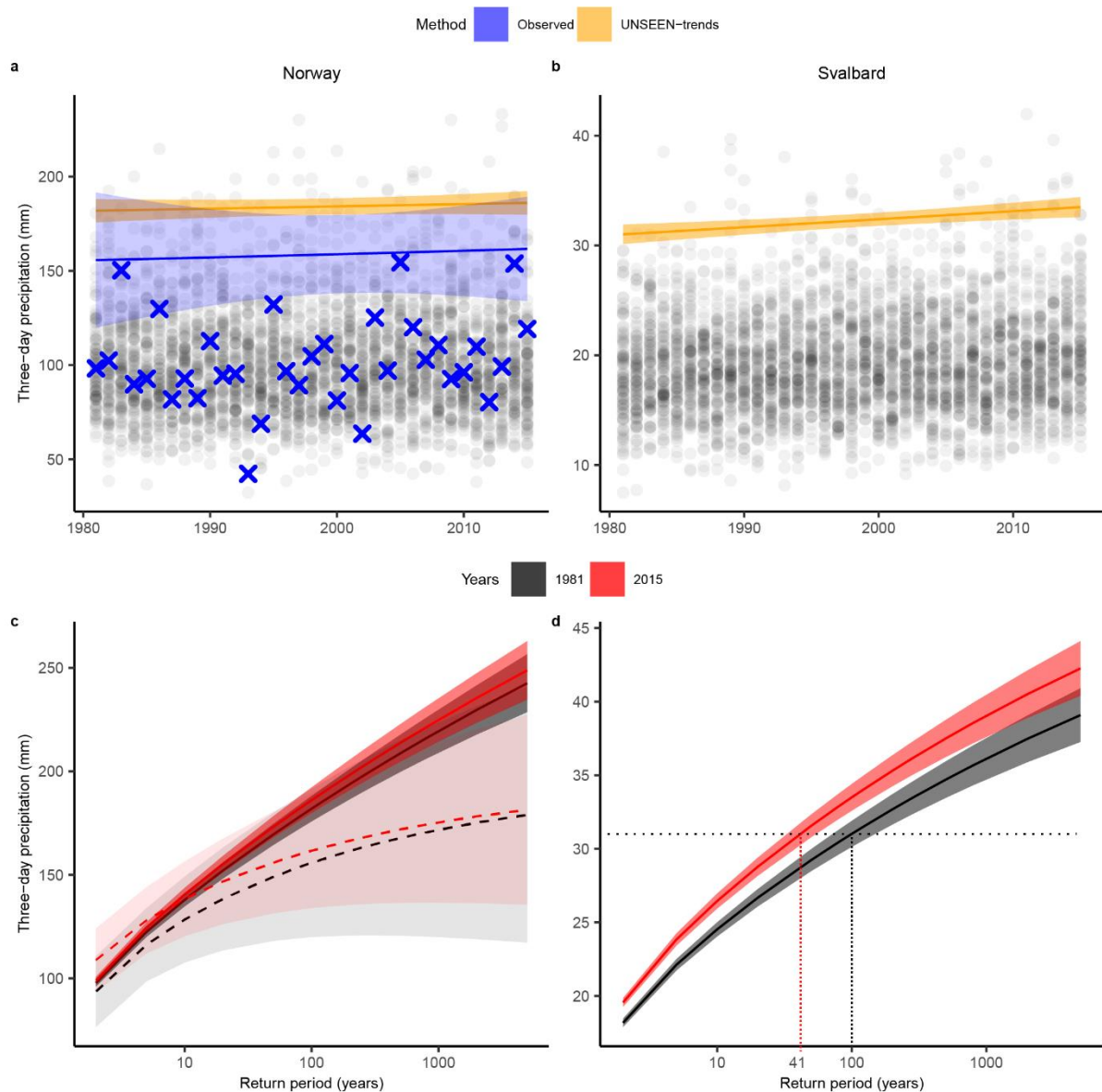
617

618 **Fig. 3 | The extreme precipitation distribution for UNSEEN and UNSEEN-BC, as compared to the**  
 619 **precipitation record over Western Norway.** The data points show the SON-3DP events and the solid  
 620 lines show the GEV fitted to the data, including 95% confidence intervals.

621

622

623



624

625 **Fig. 4 | UNSEEN-trends in extreme precipitation, as compared to trend analysis based on the**  
 626 **precipitation record. a,b,** The change in 100-year SON-3DP over 1981-2015 is shown for (a) Western  
 627 Norway and (b) Svalbard. The data points show the SON-3DP events in the observed record (blue  
 628 crosses) and in the UNSEEN-ensemble (black circles). Note, for Svalbard no gridded precipitation  
 629 record is available and for Norway the bias-corrected UNSEEN-BC is used. **c,d,** In addition to the  
 630 change in 100-year precipitation, the entire GEV distribution is plotted for the covariates 1981 and  
 631 2015 over (c) Western Norway and (d) Svalbard. Solid lines and dark shading indicate the trend and  
 632 uncertainty of the UNSEEN-trends approach and dashed lines with light shading (in c) indicates the  
 633 trend and uncertainty range based on observations. In d, the magnitude of the event with a return  
 634 period of 100 years in 1981 is illustrated with black dotted lines and the event of similar magnitude  
 635 corresponding to a return period of 41 years in 2015 is illustrated with a red dotted line.